



CERN-PH-EP-2012-091
 LHCb-PAPER-2011-022
 5 April 2012

Measurements of the branching fractions of the decays $B_s^0 \rightarrow D_s^\mp K^\pm$ and $B_s^0 \rightarrow D_s^- \pi^+$

LHCb collaboration [†]

Abstract

The decay mode $B_s^0 \rightarrow D_s^\mp K^\pm$ allows for one of the theoretically cleanest measurements of the CKM angle γ through the study of time-dependent CP violation. This paper reports a measurement of its branching fraction relative to the Cabibbo-favoured mode $B_s^0 \rightarrow D_s^- \pi^+$ based on a data sample of 0.37 fb^{-1} proton-proton collisions at $\sqrt{s} = 7 \text{ TeV}$ collected in 2011 with the LHCb detector. In addition, the ratio of B meson production fractions f_s/f_d , determined from semileptonic decays, together with the known branching fraction of the control channel $B^0 \rightarrow D^- \pi^+$, is used to perform an absolute measurement of the branching fractions:

$$\mathcal{B}(B_s^0 \rightarrow D_s^- \pi^+) = (2.95 \pm 0.05 \pm 0.17_{-0.22}^{+0.18}) \times 10^{-3},$$

$$\mathcal{B}(B_s^0 \rightarrow D_s^\mp K^\pm) = (1.90 \pm 0.12 \pm 0.13_{-0.14}^{+0.12}) \times 10^{-4},$$

where the first uncertainty is statistical, the second the experimental systematic uncertainty, and the third the uncertainty due to f_s/f_d .

Submitted to JHEP

[†]Authors are listed on the following pages.

LHCb collaboration

R. Aaij³⁸, C. Abellan Beteta^{33,n}, B. Adeva³⁴, M. Adinolfi⁴³, C. Adrover⁶, A. Affolder⁴⁹, Z. Ajaltouni⁵, J. Albrecht³⁵, F. Alessio³⁵, M. Alexander⁴⁸, S. Ali³⁸, G. Alkhazov²⁷, P. Alvarez Cartelle³⁴, A.A. Alves Jr²², S. Amato², Y. Amhis³⁶, J. Anderson³⁷, R.B. Appleby⁵¹, O. Aquines Gutierrez¹⁰, F. Archilli^{18,35}, A. Artamonov³², M. Artuso^{53,35}, E. Aslanides⁶, G. Auriemma^{22,m}, S. Bachmann¹¹, J.J. Back⁴⁵, V. Balagura^{28,35}, W. Baldini¹⁶, R.J. Barlow⁵¹, C. Barschel³⁵, S. Barsuk⁷, W. Barter⁴⁴, A. Bates⁴⁸, C. Bauer¹⁰, Th. Bauer³⁸, A. Bay³⁶, I. Bediaga¹, S. Belogurov²⁸, K. Belous³², I. Belyaev²⁸, E. Ben-Haim⁸, M. Benayoun⁸, G. Bencivenni¹⁸, S. Benson⁴⁷, J. Benton⁴³, R. Bernet³⁷, M.-O. Bettler¹⁷, M. van Beuzekom³⁸, A. Bien¹¹, S. Bifani¹², T. Bird⁵¹, A. Bizzeti^{17,h}, P.M. Bjørnstad⁵¹, T. Blake³⁵, F. Blanc³⁶, C. Blanks⁵⁰, J. Blouw¹¹, S. Blusk⁵³, A. Bobrov³¹, V. Bocci²², A. Bondar³¹, N. Bondar²⁷, W. Bonivento¹⁵, S. Borghi^{48,51}, A. Borgia⁵³, T.J.V. Bowcock⁴⁹, C. Bozzi¹⁶, T. Brambach⁹, J. van den Brand³⁹, J. Bressieux³⁶, D. Brett⁵¹, M. Britsch¹⁰, T. Britton⁵³, N.H. Brook⁴³, H. Brown⁴⁹, A. Büchler-Germann³⁷, I. Burducea²⁶, A. Bursche³⁷, J. Buytaert³⁵, S. Cadeddu¹⁵, O. Callot⁷, M. Calvi^{20,j}, M. Calvo Gomez^{33,n}, A. Camboni³³, P. Campana^{18,35}, A. Carbone¹⁴, G. Carboni^{21,k}, R. Cardinale^{19,i,35}, A. Cardini¹⁵, L. Carson⁵⁰, K. Carvalho Akiba², G. Casse⁴⁹, M. Cattaneo³⁵, Ch. Cauet⁹, M. Charles⁵², Ph. Charpentier³⁵, N. Chiapolini³⁷, K. Ciba³⁵, X. Cid Vidal³⁴, G. Ciezarek⁵⁰, P.E.L. Clarke⁴⁷, M. Clemencic³⁵, H.V. Cliff⁴⁴, J. Closier³⁵, C. Coca²⁶, V. Coco³⁸, J. Cogan⁶, P. Collins³⁵, A. Comerma-Montells³³, A. Contu⁵², A. Cook⁴³, M. Coombes⁴³, G. Corti³⁵, B. Couturier³⁵, G.A. Cowan³⁶, R. Currie⁴⁷, C. D'Ambrosio³⁵, P. David⁸, P.N.Y. David³⁸, I. De Bonis⁴, K. De Bruyn³⁸, S. De Capua^{21,k}, M. De Cian³⁷, J.M. De Miranda¹, L. De Paula², P. De Simone¹⁸, D. Decamp⁴, M. Deckenhoff⁹, H. Degaudenzi^{36,35}, L. Del Buono⁸, C. Deplano¹⁵, D. Derkach^{14,35}, O. Deschamps⁵, F. Dettori³⁹, J. Dickens⁴⁴, H. Dijkstra³⁵, P. Diniz Batista¹, F. Domingo Bonal^{33,n}, S. Donleavy⁴⁹, F. Dordei¹¹, A. Dosil Suárez³⁴, D. Dossett⁴⁵, A. Dovbnya⁴⁰, F. Dupertuis³⁶, R. Dzhelyadin³², A. Dziurda²³, S. Easo⁴⁶, U. Egede⁵⁰, V. Egorychev²⁸, S. Eidelman³¹, D. van Eijk³⁸, F. Eisele¹¹, S. Eisenhardt⁴⁷, R. Ekelhof⁹, L. Eklund⁴⁸, Ch. Elsasser³⁷, D. Elsby⁴², D. Esperante Pereira³⁴, A. Falabella^{16,e,14}, C. Färber¹¹, G. Fardell⁴⁷, C. Farinelli³⁸, S. Farry¹², V. Fave³⁶, V. Fernandez Albor³⁴, M. Ferro-Luzzi³⁵, S. Filippov³⁰, C. Fitzpatrick⁴⁷, M. Fontana¹⁰, F. Fontanelli^{19,i}, R. Forty³⁵, O. Francisco², M. Frank³⁵, C. Frei³⁵, M. Frosini^{17,f}, S. Furcas²⁰, A. Gallas Torreira³⁴, D. Galli^{14,c}, M. Gandelman², P. Gandini⁵², Y. Gao³, J.-C. Garnier³⁵, J. Garofoli⁵³, J. Garra Tico⁴⁴, L. Garrido³³, D. Gascon³³, C. Gaspar³⁵, R. Gauld⁵², N. Gauvin³⁶, M. Gersabeck³⁵, T. Gershon^{45,35}, Ph. Ghez⁴, V. Gibson⁴⁴, V.V. Gligorov³⁵, C. Göbel⁵⁴, D. Golubkov²⁸, A. Golutvin^{50,28,35}, A. Gomes², H. Gordon⁵², M. Grabalosa Gándara³³, R. Graciani Diaz³³, L.A. Granado Cardoso³⁵, E. Graugés³³, G. Graziani¹⁷, A. Grecu²⁶, E. Greening⁵², S. Gregson⁴⁴, B. Gui⁵³, E. Gushchin³⁰, Yu. Guz³², T. Gys³⁵, C. Hadjivasiliou⁵³, G. Haefeli³⁶, C. Haen³⁵, S.C. Haines⁴⁴, T. Hampson⁴³, S. Hansmann-Menzemer¹¹, R. Harji⁵⁰, N. Harnew⁵², J. Harrison⁵¹, P.F. Harrison⁴⁵, T. Hartmann⁵⁵, J. He⁷, V. Heijne³⁸, K. Hennessy⁴⁹, P. Henrard⁵, J.A. Hernando Morata³⁴, E. van Herwijnen³⁵, E. Hicks⁴⁹, K. Holubyev¹¹, P. Hopchev⁴, W. Hulsbergen³⁸, P. Hunt⁵², T. Huse⁴⁹, R.S. Huston¹², D. Hutchcroft⁴⁹, D. Hynds⁴⁸, V. Iakovenko⁴¹, P. Ilten¹², J. Imong⁴³, R. Jacobsson³⁵, A. Jaeger¹¹, M. Jahjah Hussein⁵, E. Jans³⁸, F. Jansen³⁸, P. Jaton³⁶, B. Jean-Marie⁷, F. Jing³, M. John⁵², D. Johnson⁵², C.R. Jones⁴⁴, B. Jost³⁵, M. Kaballo⁹, S. Kandybei⁴⁰, M. Karacson³⁵, T.M. Karbach⁹, J. Keaveney¹², I.R. Kenyon⁴², U. Kerzel³⁵, T. Ketel³⁹, A. Keune³⁶, B. Khanji⁶, Y.M. Kim⁴⁷, M. Knecht³⁶, R.F. Koopman³⁹,

P. Koppenburg³⁸, M. Korolev²⁹, A. Kozlinskiy³⁸, L. Kravchuk³⁰, K. Kreplin¹¹, M. Kreps⁴⁵,
 G. Krocker¹¹, P. Krovovny³¹, F. Kruse⁹, K. Kruzelecki³⁵, M. Kucharczyk^{20,23,35,j},
 V. Kudryavtsev³¹, T. Kvaratskheliya^{28,35}, V.N. La Thi³⁶, D. Lacarrere³⁵, G. Lafferty⁵¹,
 A. Lai¹⁵, D. Lambert⁴⁷, R.W. Lambert³⁹, E. Lanciotti³⁵, G. Lanfranchi¹⁸, C. Langenbruch³⁵,
 T. Latham⁴⁵, C. Lazzeroni⁴², R. Le Gac⁶, J. van Leerdam³⁸, J.-P. Lees⁴, R. Lefèvre⁵,
 A. Leflat^{29,35}, J. Lefrançois⁷, O. Leroy⁶, T. Lesiak²³, L. Li³, L. Li Gioi⁵, M. Lieng⁹, M. Liles⁴⁹,
 R. Lindner³⁵, C. Linn¹¹, B. Liu³, G. Liu³⁵, J. von Loeben²⁰, J.H. Lopes², E. Lopez Asamar³³,
 N. Lopez-March³⁶, H. Lu³, J. Luisier³⁶, A. Mac Raighne⁴⁸, F. Machefert⁷,
 I.V. Machikhiliyan^{4,28}, F. Maciuc¹⁰, O. Maev^{27,35}, J. Magnin¹, S. Malde⁵²,
 R.M.D. Mamunur³⁵, G. Manca^{15,d}, G. Mancinelli⁶, N. Mangiafave⁴⁴, U. Marconi¹⁴,
 R. Märki³⁶, J. Marks¹¹, G. Martellotti²², A. Martens⁸, L. Martin⁵², A. Martín Sánchez⁷,
 M. Martinelli³⁸, D. Martinez Santos³⁵, A. Massafferri¹, Z. Mathe¹², C. Matteuzzi²⁰,
 M. Matveev²⁷, E. Maurice⁶, B. Maynard⁵³, A. Mazurov^{16,30,35}, G. McGregor⁵¹, R. McNulty¹²,
 M. Meissner¹¹, M. Merk³⁸, J. Merkel⁹, S. Miglioranzi³⁵, D.A. Milanese¹³, M.-N. Minard⁴,
 J. Molina Rodriguez⁵⁴, S. Monteil⁵, D. Moran¹², P. Morawski²³, R. Mountain⁵³, I. Mous³⁸,
 F. Muheim⁴⁷, K. Müller³⁷, R. Muresan²⁶, B. Muryn²⁴, B. Muster³⁶, J. Mylroie-Smith⁴⁹,
 P. Naik⁴³, T. Nakada³⁶, R. Nandakumar⁴⁶, I. Nasteva¹, M. Needham⁴⁷, N. Neufeld³⁵,
 A.D. Nguyen³⁶, C. Nguyen-Mau^{36,o}, M. Nicol⁷, V. Niess⁵, N. Nikitin²⁹, T. Nikodem¹¹,
 A. Nomerotski^{52,35}, A. Novoselov³², A. Oblakowska-Mucha²⁴, V. Obraztsov³², S. Oggero³⁸,
 S. Ogilvy⁴⁸, O. Okhrimenko⁴¹, R. Oldeman^{15,d,35}, M. Orlandea²⁶, J.M. Otorola Goicochea²,
 P. Owen⁵⁰, B.K. Pal⁵³, J. Palacios³⁷, A. Palano^{13,b}, M. Palutan¹⁸, J. Panman³⁵,
 A. Papanestis⁴⁶, M. Pappagallo⁴⁸, C. Parkes⁵¹, C.J. Parkinson⁵⁰, G. Passaleva¹⁷, G.D. Patel⁴⁹,
 M. Patel⁵⁰, S.K. Paterson⁵⁰, G.N. Patrick⁴⁶, C. Patrignani^{19,i}, C. Pavel-Nicorescu²⁶,
 A. Pazos Alvarez³⁴, A. Pellegrino³⁸, G. Penso^{22,l}, M. Pepe Altarelli³⁵, S. Perazzini^{14,c},
 D.L. Perego^{20,j}, E. Perez Trigo³⁴, A. Pérez-Calero Yzquierdo³³, P. Perret⁵, M. Perrin-Terrin⁶,
 G. Pessina²⁰, A. Petrolini^{19,i}, A. Phan⁵³, E. Picatoste Olloqui³³, B. Pie Valls³³, B. Pietrzyk⁴,
 T. Pilar⁴⁵, D. Pinci²², R. Plackett⁴⁸, S. Playfer⁴⁷, M. Plo Casasus³⁴, G. Polok²³,
 A. Poluektov^{45,31}, E. Polycarpo², D. Popov¹⁰, B. Popovici²⁶, C. Potterat³³, A. Powell⁵²,
 J. Prisciandaro³⁶, V. Pugatch⁴¹, A. Puig Navarro³³, W. Qian⁵³, J.H. Rademacker⁴³,
 B. Rakotomiamanana³⁶, M.S. Rangel², I. Raniuk⁴⁰, G. Raven³⁹, S. Redford⁵², M.M. Reid⁴⁵,
 A.C. dos Reis¹, S. Ricciardi⁴⁶, A. Richards⁵⁰, K. Rinnert⁴⁹, D.A. Roa Romero⁵, P. Robbe⁷,
 E. Rodrigues^{48,51}, F. Rodrigues², P. Rodriguez Perez³⁴, G.J. Rogers⁴⁴, S. Roiser³⁵,
 V. Romanovsky³², M. Rosello^{33,n}, J. Rouvinet³⁶, T. Ruf³⁵, H. Ruiz³³, G. Sabatino^{21,k},
 J.J. Saborido Silva³⁴, N. Sagidova²⁷, P. Sail⁴⁸, B. Saitta^{15,d}, C. Salzmann³⁷, M. Sannino^{19,i},
 R. Santacesaria²², C. Santamarina Rios³⁴, R. Santinelli³⁵, E. Santovetti^{21,k}, M. Sapunov⁶,
 A. Sarti^{18,l}, C. Satriano^{22,m}, A. Satta²¹, M. Savrie^{16,e}, D. Savrina²⁸, P. Schaack⁵⁰,
 M. Schiller³⁹, H. Schindler³⁵, S. Schleich⁹, M. Schlupp⁹, M. Schmelling¹⁰, B. Schmidt³⁵,
 O. Schneider³⁶, A. Schopper³⁵, M.-H. Schune⁷, R. Schwemmer³⁵, B. Sciascia¹⁸, A. Sciubba^{18,l},
 M. Seco³⁴, A. Semennikov²⁸, K. Senderowska²⁴, I. Sepp⁵⁰, N. Serra³⁷, J. Serrano⁶, P. Seyfert¹¹,
 M. Shapkin³², I. Shapoval^{40,35}, P. Shatalov²⁸, Y. Shcheglov²⁷, T. Shears⁴⁹, L. Shekhtman³¹,
 O. Shevchenko⁴⁰, V. Shevchenko²⁸, A. Shires⁵⁰, R. Silva Coutinho⁴⁵, T. Skwarnicki⁵³,
 N.A. Smith⁴⁹, E. Smith^{52,46}, K. Sobczak⁵, F.J.P. Soler⁴⁸, A. Solomin⁴³, F. Soomro^{18,35},
 B. Souza De Paula², B. Spaan⁹, A. Sparkes⁴⁷, P. Spradlin⁴⁸, F. Stagni³⁵, S. Stahl¹¹,
 O. Steinkamp³⁷, S. Stoica²⁶, S. Stone^{53,35}, B. Storaci³⁸, M. Straticiuc²⁶, U. Straumann³⁷,
 V.K. Subbiah³⁵, S. Swientek⁹, M. Szczekowski²⁵, P. Szczypka³⁶, T. Szumlak²⁴, S. T'Jampens⁴,
 E. Teodorescu²⁶, F. Teubert³⁵, C. Thomas⁵², E. Thomas³⁵, J. van Tilburg¹¹, V. Tisserand⁴,

M. Tobin³⁷, S. Tolk³⁹, S. Topp-Joergensen⁵², N. Torr⁵², E. Tournefier^{4,50}, S. Tourneur³⁶, M.T. Tran³⁶, A. Tsaregorodtsev⁶, N. Tuning³⁸, M. Ubeda Garcia³⁵, A. Ukleja²⁵, U. Uwer¹¹, V. Vagnoni¹⁴, G. Valenti¹⁴, R. Vazquez Gomez³³, P. Vazquez Regueiro³⁴, S. Vecchi¹⁶, J.J. Velthuis⁴³, M. Veltri^{17,g}, B. Viaud⁷, I. Videau⁷, D. Vieira², X. Vilasis-Cardona^{33,n}, J. Visniakov³⁴, A. Vollhardt³⁷, D. Volyanskyy¹⁰, D. Voong⁴³, A. Vorobyev²⁷, V. Vorobyev³¹, H. Voss¹⁰, R. Waldi⁵⁵, S. Wandernoth¹¹, J. Wang⁵³, D.R. Ward⁴⁴, N.K. Watson⁴², A.D. Webber⁵¹, D. Websdale⁵⁰, M. Whitehead⁴⁵, D. Wiedner¹¹, L. Wiggers³⁸, G. Wilkinson⁵², M.P. Williams^{45,46}, M. Williams⁵⁰, F.F. Wilson⁴⁶, J. Wishahi⁹, M. Witek²³, W. Witzeling³⁵, S.A. Wotton⁴⁴, K. Wyllie³⁵, Y. Xie⁴⁷, F. Xing⁵², Z. Xing⁵³, Z. Yang³, R. Young⁴⁷, O. Yushchenko³², M. Zangoli¹⁴, M. Zavertyaev^{10,a}, F. Zhang³, L. Zhang⁵³, W.C. Zhang¹², Y. Zhang³, A. Zhelezov¹¹, L. Zhong³, A. Zvyagin³⁵.

¹ *Centro Brasileiro de Pesquisas Físicas (CBPF), Rio de Janeiro, Brazil*

² *Universidade Federal do Rio de Janeiro (UFRJ), Rio de Janeiro, Brazil*

³ *Center for High Energy Physics, Tsinghua University, Beijing, China*

⁴ *LAPP, Université de Savoie, CNRS/IN2P3, Annecy-Le-Vieux, France*

⁵ *Clermont Université, Université Blaise Pascal, CNRS/IN2P3, LPC, Clermont-Ferrand, France*

⁶ *CPPM, Aix-Marseille Université, CNRS/IN2P3, Marseille, France*

⁷ *LAL, Université Paris-Sud, CNRS/IN2P3, Orsay, France*

⁸ *LPNHE, Université Pierre et Marie Curie, Université Paris Diderot, CNRS/IN2P3, Paris, France*

⁹ *Fakultät Physik, Technische Universität Dortmund, Dortmund, Germany*

¹⁰ *Max-Planck-Institut für Kernphysik (MPIK), Heidelberg, Germany*

¹¹ *Physikalisches Institut, Ruprecht-Karls-Universität Heidelberg, Heidelberg, Germany*

¹² *School of Physics, University College Dublin, Dublin, Ireland*

¹³ *Sezione INFN di Bari, Bari, Italy*

¹⁴ *Sezione INFN di Bologna, Bologna, Italy*

¹⁵ *Sezione INFN di Cagliari, Cagliari, Italy*

¹⁶ *Sezione INFN di Ferrara, Ferrara, Italy*

¹⁷ *Sezione INFN di Firenze, Firenze, Italy*

¹⁸ *Laboratori Nazionali dell'INFN di Frascati, Frascati, Italy*

¹⁹ *Sezione INFN di Genova, Genova, Italy*

²⁰ *Sezione INFN di Milano Bicocca, Milano, Italy*

²¹ *Sezione INFN di Roma Tor Vergata, Roma, Italy*

²² *Sezione INFN di Roma La Sapienza, Roma, Italy*

²³ *Henryk Niewodniczanski Institute of Nuclear Physics Polish Academy of Sciences, Kraków, Poland*

²⁴ *AGH University of Science and Technology, Kraków, Poland*

²⁵ *Soltan Institute for Nuclear Studies, Warsaw, Poland*

²⁶ *Horia Hulubei National Institute of Physics and Nuclear Engineering, Bucharest-Magurele, Romania*

²⁷ *Petersburg Nuclear Physics Institute (PNPI), Gatchina, Russia*

²⁸ *Institute of Theoretical and Experimental Physics (ITEP), Moscow, Russia*

²⁹ *Institute of Nuclear Physics, Moscow State University (SINP MSU), Moscow, Russia*

³⁰ *Institute for Nuclear Research of the Russian Academy of Sciences (INR RAN), Moscow, Russia*

³¹ *Budker Institute of Nuclear Physics (SB RAS) and Novosibirsk State University, Novosibirsk, Russia*

³² *Institute for High Energy Physics (IHEP), Protvino, Russia*

³³ *Universitat de Barcelona, Barcelona, Spain*

³⁴ *Universidad de Santiago de Compostela, Santiago de Compostela, Spain*

³⁵ *European Organization for Nuclear Research (CERN), Geneva, Switzerland*

³⁶ *Ecole Polytechnique Fédérale de Lausanne (EPFL), Lausanne, Switzerland*

³⁷ *Physik-Institut, Universität Zürich, Zürich, Switzerland*

³⁸ *Nikhef National Institute for Subatomic Physics, Amsterdam, The Netherlands*

³⁹ *Nikhef National Institute for Subatomic Physics and VU University Amsterdam, Amsterdam, The Netherlands*

Netherlands

⁴⁰ *NSC Kharkiv Institute of Physics and Technology (NSC KIPT), Kharkiv, Ukraine*

⁴¹ *Institute for Nuclear Research of the National Academy of Sciences (KINR), Kyiv, Ukraine*

⁴² *University of Birmingham, Birmingham, United Kingdom*

⁴³ *H.H. Wills Physics Laboratory, University of Bristol, Bristol, United Kingdom*

⁴⁴ *Cavendish Laboratory, University of Cambridge, Cambridge, United Kingdom*

⁴⁵ *Department of Physics, University of Warwick, Coventry, United Kingdom*

⁴⁶ *STFC Rutherford Appleton Laboratory, Didcot, United Kingdom*

⁴⁷ *School of Physics and Astronomy, University of Edinburgh, Edinburgh, United Kingdom*

⁴⁸ *School of Physics and Astronomy, University of Glasgow, Glasgow, United Kingdom*

⁴⁹ *Oliver Lodge Laboratory, University of Liverpool, Liverpool, United Kingdom*

⁵⁰ *Imperial College London, London, United Kingdom*

⁵¹ *School of Physics and Astronomy, University of Manchester, Manchester, United Kingdom*

⁵² *Department of Physics, University of Oxford, Oxford, United Kingdom*

⁵³ *Syracuse University, Syracuse, NY, United States*

⁵⁴ *Pontificia Universidade Católica do Rio de Janeiro (PUC-Rio), Rio de Janeiro, Brazil, associated to ²*

⁵⁵ *Institut für Physik, Universität Rostock, Rostock, Germany, associated to ¹¹*

^a *P.N. Lebedev Physical Institute, Russian Academy of Science (LPI RAS), Moscow, Russia*

^b *Università di Bari, Bari, Italy*

^c *Università di Bologna, Bologna, Italy*

^d *Università di Cagliari, Cagliari, Italy*

^e *Università di Ferrara, Ferrara, Italy*

^f *Università di Firenze, Firenze, Italy*

^g *Università di Urbino, Urbino, Italy*

^h *Università di Modena e Reggio Emilia, Modena, Italy*

ⁱ *Università di Genova, Genova, Italy*

^j *Università di Milano Bicocca, Milano, Italy*

^k *Università di Roma Tor Vergata, Roma, Italy*

^l *Università di Roma La Sapienza, Roma, Italy*

^m *Università della Basilicata, Potenza, Italy*

ⁿ *LIFAEELS, La Salle, Universitat Ramon Llull, Barcelona, Spain*

^o *Hanoi University of Science, Hanoi, Viet Nam*

1 Introduction

Unlike the flavour-specific decay $B_s^0 \rightarrow D_s^- \pi^+$, the Cabibbo-suppressed decay $B_s^0 \rightarrow D_s^\mp K^\pm$ proceeds through two different tree-level amplitudes of similar strength: a $\bar{b} \rightarrow \bar{c} u \bar{s}$ transition leading to $B_s^0 \rightarrow D_s^- K^+$ and a $\bar{b} \rightarrow \bar{u} c \bar{s}$ transition leading to $B_s^0 \rightarrow D_s^+ K^-$. These two decay amplitudes can have a large CP -violating interference via $B_s^0 - \bar{B}_s^0$ mixing, allowing the determination of the CKM angle γ with negligible theoretical uncertainties through the measurement of tagged and untagged time-dependent decay rates to both the $D_s^- K^+$ and $D_s^+ K^-$ final states [1]. Although the $B_s^0 \rightarrow D_s^\mp K^\pm$ decay mode has been observed by the CDF [2] and BELLE [3] collaborations, only the LHCb experiment has both the necessary decay time resolution and access to large enough signal yields to perform the time-dependent CP measurement. In this analysis, the $B_s^0 \rightarrow D_s^\mp K^\pm$ branching fraction is determined relative to $B_s^0 \rightarrow D_s^- \pi^+$, and the absolute $B_s^0 \rightarrow D_s^- \pi^+$ branching fraction is determined using the known branching fraction of $B^0 \rightarrow D^- \pi^+$ and the production fraction ratio f_s/f_d [4]. The two measurements are then combined to obtain the absolute branching fraction of the decay $B_s^0 \rightarrow D_s^\mp K^\pm$. Charge conjugate modes are implied throughout. Our notation $B^0 \rightarrow D^- \pi^+$, which matches that of Ref. [5], encompasses both the Cabibbo-favoured $B^0 \rightarrow D^- \pi^+$ mode and the doubly-Cabibbo-suppressed $B^0 \rightarrow D^+ \pi^-$ mode.

The LHCb detector [6] is a single-arm forward spectrometer covering the pseudo-rapidity range $2 < \eta < 5$, designed for studying particles containing b or c quarks. The detector includes a high-precision tracking system consisting of a silicon-strip vertex detector surrounding the pp interaction region, a large-area silicon-strip detector located upstream of a dipole magnet with a bending power of about 4 Tm, and three stations of silicon-strip detectors and straw drift tubes placed downstream. The combined tracking system has a momentum resolution $\Delta p/p$ that varies from 0.4% at 5 GeV/ c to 0.6% at 100 GeV/ c , an impact parameter resolution of 20 μm for tracks with high transverse momentum, and a decay time resolution of 50 fs. Charged hadrons are identified using two ring-imaging Cherenkov detectors. Photon, electron and hadron candidates are identified by a calorimeter system consisting of scintillating-pad and pre-shower detectors, an electromagnetic calorimeter, and a hadronic calorimeter. Muons are identified by a muon system composed of alternating layers of iron and multiwire proportional chambers.

The LHCb trigger consists of a hardware stage, based on information from the calorimeter and muon systems, followed by a software stage which applies a full event reconstruction. Two categories of events are recognised based on the hardware trigger decision. The first category are events triggered by tracks from signal decays which have an associated cluster in the calorimeters, and the second category are events triggered independently of the signal decay particles. Events which do not fall into either of these two categories are not used in the subsequent analysis. The second, software, trigger stage requires a two-, three- or four-track secondary vertex with a large value of the scalar sum of the transverse momenta (p_T) of the tracks, and a significant displacement from the primary interaction. At least one of the tracks used to form this vertex is required to have $p_T > 1.7$ GeV/ c , an impact parameter $\chi^2 > 16$, and a track fit χ^2 per degree of free-

dom $\chi^2/\text{ndf} < 2$. A multivariate algorithm is used for the identification of the secondary vertices [7]. Each input variable is binned to minimise the effect of systematic differences between the trigger behaviour on data and simulated events.

The samples of simulated events used in this analysis are based on the PYTHIA 6.4 generator [8], with a choice of parameters specifically configured for LHCb [9]. The EVTGEN package [10] describes the decay of the B mesons, and the GEANT4 package [11] simulates the detector response. QED radiative corrections are generated with the PHOTOS package [12].

The analysis is based on a sample of pp collisions corresponding to an integrated luminosity of 0.37 fb^{-1} , collected at the LHC in 2011 at a centre-of-mass energy $\sqrt{s} = 7 \text{ TeV}$. The decay modes $B_s^0 \rightarrow D_s^- \pi^+$ and $B_s^0 \rightarrow D_s^\mp K^\pm$ are topologically identical and are selected using identical geometric and kinematic criteria, thereby minimising efficiency corrections in the ratio of branching fractions. The decay mode $B^0 \rightarrow D^- \pi^+$ has a similar topology to the other two, differing only in the Dalitz plot structure of the D decay and the lifetime of the D meson. These differences are verified, using simulated events, to alter the selection efficiency at the level of a few percent, and are taken into account.

B_s^0 (B^0) candidates are reconstructed from a D_s^- (D^-) candidate and an additional pion or kaon (the ‘‘bachelor’’ particle), with the D_s^- (D^-) meson decaying in the $K^+ K^- \pi^-$ ($K^+ \pi^- \pi^-$) mode. All selection criteria will now be specified for the B_s^0 decays, and are implied to be identical for the B^0 decay unless explicitly stated otherwise. All final-state particles are required to satisfy a track fit $\chi^2/\text{ndf} < 4$ and to have a high transverse momentum and a large impact parameter χ^2 with respect to all primary vertices in the event. In order to remove backgrounds which contain the same final-state particles as the signal decay, and therefore have the same mass lineshape, but do not proceed through the decay of a charmed meson, the flight distance χ^2 of the D_s^- from the B_s^0 is required to be larger than 2. Only D_s^- and bachelor candidates forming a vertex with a $\chi^2/\text{ndf} < 9$ are considered as B_s^0 candidates. The same vertex quality criterion is applied to the D_s^- candidates. The B_s^0 candidate is further required to point to the primary vertex imposing $\theta_{\text{flight}} < 0.8$ degrees, where θ_{flight} is the angle between the candidate momentum vector and the line between the primary vertex and the B_s^0 vertex. The B_s^0 candidates are also required to have a χ^2 of their impact parameter with respect to the primary vertex less than 16.

Further suppression of combinatorial backgrounds is achieved using a gradient boosted decision tree technique [13] identical to the decision tree used in the previously published determination of f_s/f_d with the hadronic decays [14]. The optimal working point is evaluated directly from a sub-sample of $B_s^0 \rightarrow D_s^- \pi^+$ events, corresponding to 10% of the full dataset used, distributed evenly over the data taking period and selected using particle identification and trigger requirements. The chosen figure of merit is the significance of the $B_s^0 \rightarrow D_s^\mp K^\pm$ signal, scaled according to the Cabibbo suppression relative to the $B_s^0 \rightarrow D_s^- \pi^+$ signal, with respect to the combinatorial background. The significance exhibits a wide plateau around its maximum, and the optimal working point is chosen at the point in the plateau which maximizes the signal yield. Multiple candidates occur in about 2% of the events and in such cases a single candidate is selected at random.

2 Particle identification

Particle identification (PID) criteria serve two purposes in the selection of the three signal decays $B^0 \rightarrow D^- \pi^+$, $B_s^0 \rightarrow D_s^- \pi^+$ and $B_s^0 \rightarrow D_s^\mp K^\pm$. When applied to the decay products of the D_s^- or D^- , they suppress misidentified backgrounds which have the same bachelor particle as the signal mode under consideration, henceforth the ‘‘cross-feed’’ backgrounds. When applied to the bachelor particle (pion or kaon) they separate the Cabibbo-favoured from the Cabibbo-suppressed decay modes. All PID criteria are based on the differences in log-likelihood (DLL) between the kaon, proton, or pion hypotheses. Their efficiencies are obtained from calibration samples of $D^{*+} \rightarrow (D^0 \rightarrow K^- \pi^+) \pi^+$ and $\Lambda \rightarrow p \pi^-$ signals, which are themselves selected without any PID requirements. These samples are split according to the magnet polarity, binned in momentum and p_T , and then reweighted to have the same momentum and p_T distributions as the signal decays under study.

The selection of a pure $B^0 \rightarrow D^- \pi^+$ sample can be accomplished with minimal PID requirements since all cross-feed backgrounds are less abundant than the signal. The $\bar{\Lambda}_b^0 \rightarrow \bar{\Lambda}_c^- \pi^+$ background is suppressed by requiring that both pions produced in the D^- decay satisfy $\text{DLL}_{\pi-p} > -10$, and the $B^0 \rightarrow D^- K^+$ background is suppressed by requiring that the bachelor pion satisfies $\text{DLL}_{K-\pi} < 0$.

The selection of a pure $B_s^0 \rightarrow D_s^- \pi^+$ or $B_s^0 \rightarrow D_s^\mp K^\pm$ sample requires the suppression of the $B^0 \rightarrow D^- \pi^+$ and $\bar{\Lambda}_b^0 \rightarrow \bar{\Lambda}_c^- \pi^+$ backgrounds, whereas the combinatorial background contributes to a lesser extent. The D^- contamination in the D_s^- data sample is reduced by requiring that the kaon which has the same charge as the pion in $D_s^- \rightarrow K^+ K^- \pi^-$ satisfies $\text{DLL}_{K-\pi} > 5$. In addition, the other kaon is required to satisfy $\text{DLL}_{K-\pi} > 0$. This helps to suppress combinatorial as well as doubly misidentified backgrounds. For the same reason the pion is required to have $\text{DLL}_{K-\pi} < 5$. The contamination of $\bar{\Lambda}_b^0 \rightarrow \bar{\Lambda}_c^- \pi^+$, $\bar{\Lambda}_c^- \rightarrow \bar{p} K^+ \pi^-$ is reduced by applying a requirement of $\text{DLL}_{K-p} > 0$ to the candidates that, when reconstructed under the $\bar{\Lambda}_c^- \rightarrow \bar{p} K^+ \pi^-$ mass hypothesis, lie within ± 21 MeV/ c^2 of the $\bar{\Lambda}_c^-$ mass.

Because of its larger branching fraction, $B_s^0 \rightarrow D_s^- \pi^+$ is a significant background to $B_s^0 \rightarrow D_s^\mp K^\pm$. It is suppressed by demanding that the bachelor satisfies the criterion $\text{DLL}_{K-\pi} > 5$. Conversely, a sample of $B_s^0 \rightarrow D_s^- \pi^+$, free of $B_s^0 \rightarrow D_s^\mp K^\pm$ contamination, is obtained by requiring that the bachelor satisfies $\text{DLL}_{K-\pi} < 0$. The efficiency and misidentification probabilities for the PID criterion used to select the bachelor, D^- , and D_s^- candidates are summarised in Table 1.

3 Mass fits

The fits to the invariant mass distributions of the $B_s^0 \rightarrow D_s^- \pi^+$ and $B_s^0 \rightarrow D_s^\mp K^\pm$ candidates require knowledge of the signal and background shapes. The signal lineshape is taken from a fit to simulated signal events which had the full trigger, reconstruction, and selection chain applied to them. Various lineshape parameterisations have been examined. The best fit to the simulated event distributions is obtained with the sum of two Crystal

Table 1: PID efficiency and misidentification probabilities, separated according to the up (U) and down (D) magnet polarities. The first two lines refer to the bachelor track selection, the third line is the D^- efficiency and the fourth the D_s^- efficiency. Probabilities are obtained from the efficiencies in the D^{*+} calibration sample, binned in momentum and p_T . Only bachelor tracks with momentum below 100 GeV/ c are considered. The uncertainties shown are the statistical uncertainties due to the finite number of signal events in the PID calibration samples.

	PID Cut	Efficiency (%)		Misidentification (%)	
		U	D	U	D
K	$DLL_{K-\pi} > 5$	83.3 ± 0.2	83.5 ± 0.2	5.3 ± 0.1	4.5 ± 0.1
π	$DLL_{K-\pi} < 0$	84.2 ± 0.2	85.8 ± 0.2	5.3 ± 0.1	5.4 ± 0.1
D^-		84.1 ± 0.2	85.7 ± 0.2	-	-
D_s^-		77.6 ± 0.2	78.4 ± 0.2	-	-

Ball functions [15] with a common peak position and width, and opposite side power-law tails. Mass shifts in the signal peaks relative to world average values [5], arising from an imperfect detector alignment [16], are observed in the data and are accounted for. A constraint on the D_s^- meson mass is used to improve the B_s^0 mass resolution. Three kinds of backgrounds need to be considered: fully reconstructed (misidentified) backgrounds, partially reconstructed backgrounds with or without misidentification (*e.g.* $B_s^0 \rightarrow D_s^{*-} K^+$ or $B_s^0 \rightarrow D_s^- \rho^+$), and combinatorial backgrounds.

The three most important fully reconstructed backgrounds are $B^0 \rightarrow D_s^- K^+$ and $B_s^0 \rightarrow D_s^- \pi^+$ for $B_s^0 \rightarrow D_s^\mp K^\pm$, and $B^0 \rightarrow D^- \pi^+$ for $B_s^0 \rightarrow D_s^- \pi^+$. The mass distribution of the $B^0 \rightarrow D^- \pi^+$ events does not suffer from fully reconstructed backgrounds. In the case of the $B^0 \rightarrow D_s^- K^+$ decay, which is fully reconstructed under its own mass hypothesis, the signal shape is fixed to be the same as for $B_s^0 \rightarrow D_s^\mp K^\pm$ and the peak position is varied. The shapes of the misidentified backgrounds $B^0 \rightarrow D^- \pi^+$ and $B_s^0 \rightarrow D_s^- \pi^+$ are taken from data using a reweighting procedure. First, a clean signal sample of $B^0 \rightarrow D^- \pi^+$ and $B_s^0 \rightarrow D_s^- \pi^+$ decays is obtained by applying the PID selection for the bachelor track given in Sect. 2. The invariant mass of these decays under the wrong mass hypothesis ($B_s^0 \rightarrow D_s^- \pi^+$ or $B_s^0 \rightarrow D_s^\mp K^\pm$) depends on the momentum of the misidentified particle. This momentum distribution must therefore be reweighted by taking into account the momentum dependence of the misidentification rate. This dependence is obtained using a dedicated calibration sample of prompt D^{*+} decays. The mass distributions under the wrong mass hypothesis are then reweighted using this momentum distribution to obtain the $B^0 \rightarrow D^- \pi^+$ and $B_s^0 \rightarrow D_s^- \pi^+$ mass shapes under the $B_s^0 \rightarrow D_s^- \pi^+$ and $B_s^0 \rightarrow D_s^\mp K^\pm$ mass hypotheses, respectively.

For partially reconstructed backgrounds, the probability density functions (PDFs) of the invariant mass distributions are taken from samples of simulated events generated in specific exclusive modes and are corrected for mass shifts, momentum spectra, and PID efficiencies in data. The use of simulated events is justified by the observed good

agreement between data and simulation.

The combinatorial background in the $B_s^0 \rightarrow D_s^- \pi^+$ and $B^0 \rightarrow D^- \pi^+$ fits is modelled by an exponential function where the exponent is allowed to vary in the fit. The resulting shape and normalisation of the combinatorial backgrounds are in agreement within one standard deviation with the distribution of a wrong-sign control sample (where the D_s^- and the bachelor track have the same charges). The shape of the combinatorial background in the $B_s^0 \rightarrow D_s^\mp K^\pm$ fit cannot be left free because of the partially reconstructed backgrounds which dominate in the mass region below the signal peak. In this case, therefore, the combinatorial slope is fixed to be flat, as measured from the wrong sign events.

In the $B_s^0 \rightarrow D_s^\mp K^\pm$ fit, an additional complication arises due to backgrounds from $\Lambda_b^0 \rightarrow D_s^- p$ and $\Lambda_b^0 \rightarrow D_s^{*-} p$, which fall in the signal region when misreconstructed. To avoid a loss of $B_s^0 \rightarrow D_s^\mp K^\pm$ signal, no requirement is made on the DLL_{K-p} of the bachelor particle. Instead, the $\Lambda_b^0 \rightarrow D_s^- p$ mass shape is obtained from simulated $\Lambda_b^0 \rightarrow D_s^- p$ decays, which are reweighted in momentum using the efficiency of the $\text{DLL}_{K-\pi} > 5$ requirement on protons. The $\Lambda_b^0 \rightarrow D_s^{*-} p$ mass shape is obtained by shifting the $\Lambda_b^0 \rightarrow D_s^- p$ mass shape downwards by $200 \text{ MeV}/c^2$. The branching fractions of $\Lambda_b^0 \rightarrow D_s^- p$ and $\Lambda_b^0 \rightarrow D_s^{*-} p$ are assumed to be equal, motivated by the fact that the decays $B^0 \rightarrow D^- D_s^+$ and $B^0 \rightarrow D^- D_s^{*+}$ (dominated by similar tree topologies) have almost equal branching fractions. Therefore the overall mass shape is formed by summing the $\Lambda_b^0 \rightarrow D_s^- p$ and $\Lambda_b^0 \rightarrow D_s^{*-} p$ shapes with equal weight.

The signal yields are obtained from unbinned extended maximum likelihood fits to the data. In order to achieve the highest sensitivity, the sample is separated according to the two magnet polarities, allowing for possible differences in PID performance and in running conditions. A simultaneous fit to the two magnet polarities is performed for each decay, with the peak position and width of each signal, as well as the combinatorial background shape, shared between the two.

The fit under the $B_s^0 \rightarrow D_s^- \pi^+$ hypothesis requires a description of the $B^0 \rightarrow D^- \pi^+$ background. A fit to the $B^0 \rightarrow D^- \pi^+$ spectrum is first performed to determine the yield of signal $B^0 \rightarrow D^- \pi^+$ events, shown in Fig. 1. The expected $B^0 \rightarrow D^- \pi^+$ contribution under the $B_s^0 \rightarrow D_s^- \pi^+$ hypothesis is subsequently constrained with a 10% uncertainty to account for uncertainties on the PID efficiencies. The fits to the $B_s^0 \rightarrow D_s^- \pi^+$ candidates are shown in Fig. 1 and the fit results for both decay modes are summarised in Table 2. The peak position of the signal shape is varied, as are the yields of the different partially reconstructed backgrounds (except $B^0 \rightarrow D^- \pi^+$) and the shape of the combinatorial background. The width of the signal is fixed to the values found in the $B^0 \rightarrow D^- \pi^+$ fit ($17.2 \text{ MeV}/c^2$), scaled by the ratio of widths observed in simulated events between $B^0 \rightarrow D^- \pi^+$ and $B_s^0 \rightarrow D_s^- \pi^+$ decays (0.987). The accuracy of these fixed parameters is evaluated using ensembles of simulated experiments described in Sect. 4. The yield of $B^0 \rightarrow D_s^- \pi^+$ is fixed to be 2.9% of the $B_s^0 \rightarrow D_s^- \pi^+$ signal yield, based on the world average branching fraction of $B^0 \rightarrow D_s^- \pi^+$ of $(2.16 \pm 0.26) \times 10^{-5}$, the value of f_s/f_d given in [4], and the value of the branching fraction computed in this paper. The shape used to fit this component is the sum of two Crystal Ball functions obtained from the $B_s^0 \rightarrow D_s^- \pi^+$ sample with the peak position fixed to the value obtained with the fit of the $B^0 \rightarrow D^- \pi^+$

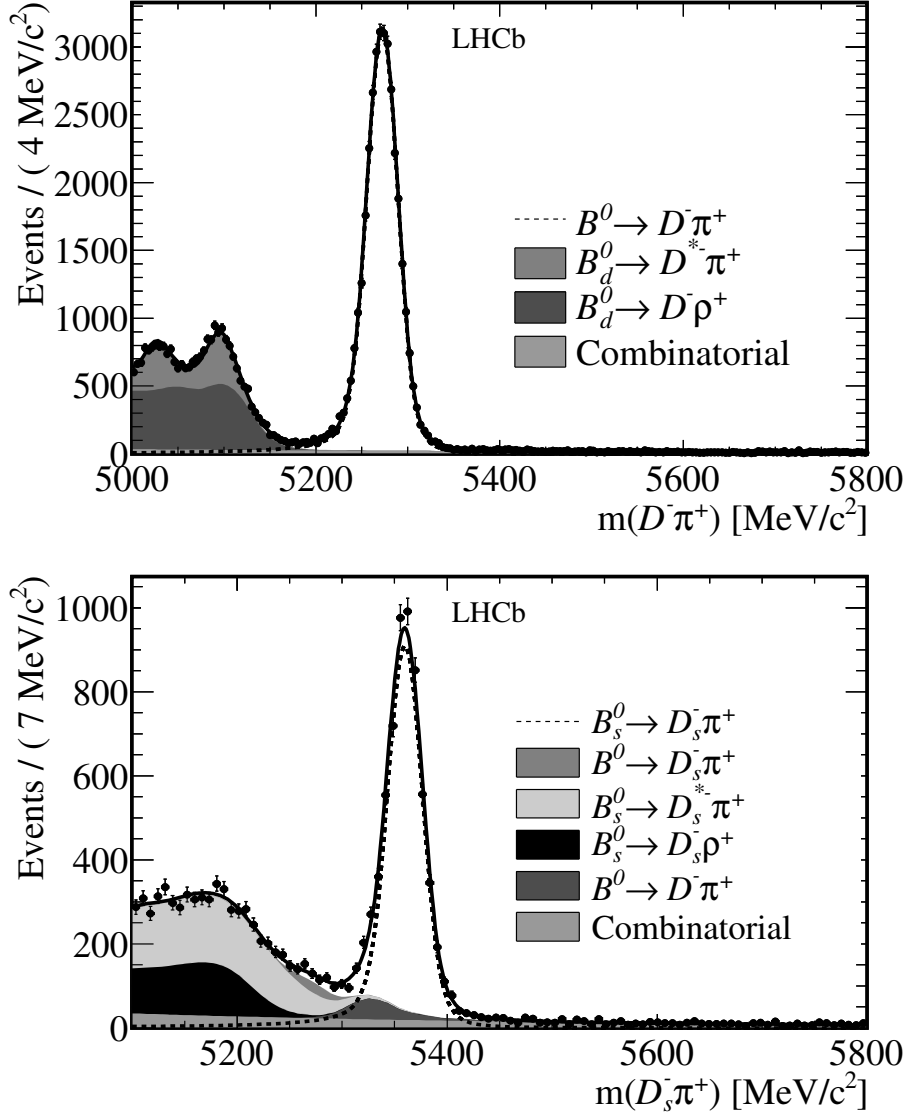


Figure 1: Mass distribution of the $B^0 \rightarrow D^- \pi^+$ candidates (top) and $B_s^0 \rightarrow D_s^- \pi^+$ candidates (bottom). The stacked background shapes follow the same top-to-bottom order in the legend and the plot. For illustration purposes the plot includes events from both magnet polarities, but they are fitted separately as described in the text.

data sample and the width fixed to the width of the $B_s^0 \rightarrow D_s^- \pi^+$ peak.

The $\bar{A}_b^0 \rightarrow \bar{A}_c^- \pi^+$ background is negligible in this fit owing to the effectiveness of the veto procedure described earlier. Nevertheless, a $\bar{A}_b^0 \rightarrow \bar{A}_c^- \pi^+$ component, whose yield is allowed to vary, is included in the fit (with the mass shape obtained using the reweighting procedure on simulated events described previously) and results in a negligible contribution, as expected.

The fits for the $B_s^0 \rightarrow D_s^\mp K^\pm$ candidates are shown in Fig. 2 and the fit results

Table 2: Results of the mass fits to the $B^0 \rightarrow D^- \pi^+$, $B_s^0 \rightarrow D_s^- \pi^+$, and $B_s^0 \rightarrow D_s^\mp K^\pm$ candidates separated according to the up (U) and down (D) magnet polarities. In the $B_s^0 \rightarrow D_s^\mp K^\pm$ case, the number quoted for $B_s^0 \rightarrow D_s^- \pi^+$ also includes a small number of $B^0 \rightarrow D^- \pi^+$ events which have the same mass shape (20 events from the expected misidentification). See Table 3 for the constrained values used in the $B_s^0 \rightarrow D_s^\mp K^\pm$ decay fit for the partially reconstructed backgrounds and the $B^0 \rightarrow D^- K^+$ decay channel.

Channel	$B^0 \rightarrow D^- \pi^+$		$B_s^0 \rightarrow D_s^- \pi^+$		$B_s^0 \rightarrow D_s^\mp K^\pm$	
	U	D	U	D	U	D
N_{Signal}	16304 ± 137	20150 ± 152	2677 ± 62	3369 ± 69	195 ± 18	209 ± 19
N_{Comb}	1922 ± 123	2049 ± 118	869 ± 63	839 ± 47	149 ± 25	255 ± 30
$N_{\text{Part-Reco}}$	10389 ± 407	12938 ± 441	2423 ± 65	3218 ± 69	-	-
$N_{B^0 \rightarrow D_s^- K^+}$	-	-	-	-	87 ± 17	100 ± 18
$N_{B_s^0 \rightarrow D_s^- \pi^+}$	-	-	-	-	154 ± 20	164 ± 22

are collected in Table 2. There are numerous reflections which contribute to the mass distribution. The most important reflection is $B_s^0 \rightarrow D_s^- \pi^+$, whose shape is taken from the earlier $B_s^0 \rightarrow D_s^- \pi^+$ signal fit, reweighted according to the efficiencies of the applied PID requirements. Furthermore, the yield of the $B^0 \rightarrow D^- K^+$ reflection is constrained to the values in Table 3. In addition, there is potential cross-feed from partially reconstructed modes with a misidentified pion such as $B_s^0 \rightarrow D_s^- \rho^+$, as well as several small contributions from partially reconstructed backgrounds with similar mass shapes. The yields of these modes, whose branching fractions are known or can be estimated (*e.g.* $B_s^0 \rightarrow D_s^- \rho^+$, $B_s^0 \rightarrow D_s^- K^{*+}$), are constrained to the values in Table 3, based on criteria such as relative branching fractions and reconstruction efficiencies and PID probabilities. An important cross-check is performed by comparing the fitted value of the yield of misidentified $B_s^0 \rightarrow D_s^- \pi^+$ events (318 ± 30) to the yield expected from PID efficiencies (370 ± 11) and an agreement is found.

4 Systematic uncertainties

The major systematic uncertainties on the measurement of the relative branching fraction of $B_s^0 \rightarrow D_s^\mp K^\pm$ and $B_s^0 \rightarrow D_s^- \pi^+$ are related to the fit, PID calibration, and trigger and offline selection efficiency corrections. Systematic uncertainties related to the fit are evaluated by generating large sets of simulated experiments using the nominal fit, and then fitting them with a model where certain parameters are varied. To give two examples, the signal width is deliberately fixed to a value different from the width used in the generation, or the combinatorial background slope in the $B_s^0 \rightarrow D_s^\mp K^\pm$ fit is fixed to the combinatorial background slope found in the $B_s^0 \rightarrow D_s^- \pi^+$ fit. The deviations of the peak position of the pull distributions from zero are then included in the systematic uncertainty.

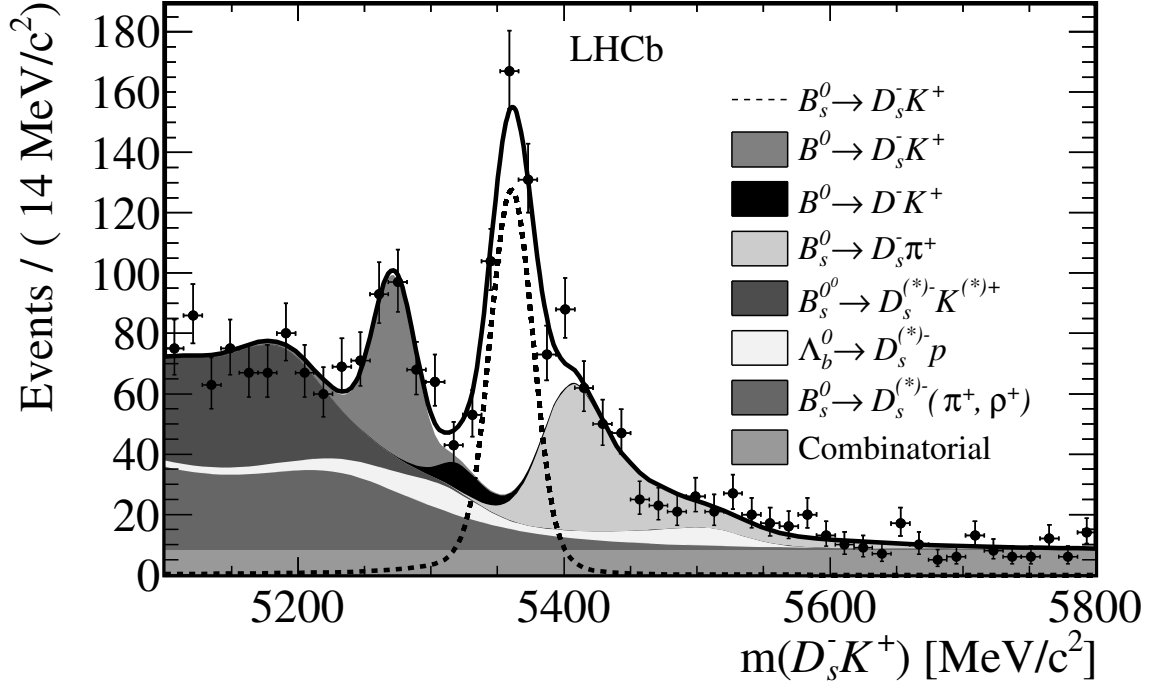


Figure 2: Mass distribution of the $B_s^0 \rightarrow D_s^\mp K^\pm$ candidates. The stacked background shapes follow the same top-to-bottom order in the legend and the plot. For illustration purposes the plot includes events from both magnet polarities, but they are fitted separately as described in the text.

In the case of the $B_s^0 \rightarrow D_s^\mp K^\pm$ fit the presence of constraints for the partially reconstructed backgrounds must be considered. The generic extended likelihood function can

Table 3: Gaussian constraints on the yields of partially reconstructed and misidentified backgrounds applied in the $B_s^0 \rightarrow D_s^\mp K^\pm$ fit, separated according to the up (U) and down (D) magnet polarities.

Background type	U	D
$B^0 \rightarrow D^- K^+$	16 ± 3	17 ± 3
$B_s^0 \rightarrow D_s^{*-} \pi^+$	63 ± 21	70 ± 23
$B_s^0 \rightarrow D_s^{*-} K^+$	72 ± 34	80 ± 27
$B_s^0 \rightarrow D_s^- \rho^+$	135 ± 45	150 ± 50
$B_s^0 \rightarrow D_s^- K^{*+}$	135 ± 45	150 ± 50
$B_s^0 \rightarrow D_s^{*-} \rho^+$	45 ± 15	50 ± 17
$B_s^0 \rightarrow D_s^{*-} K^{*+}$	45 ± 15	50 ± 17
$\Lambda_b^0 \rightarrow D_s^- p + \Lambda_b^0 \rightarrow D_s^{*-} p$	72 ± 34	80 ± 27

Table 4: Relative systematic uncertainties on the branching fraction ratios.

Source	$\frac{B_s^0 \rightarrow D_s^\mp K^\pm}{B_s^0 \rightarrow D_s^- \pi^+}$ (%)	$\frac{B_s^0 \rightarrow D_s^- \pi^+}{B^0 \rightarrow D^- \pi^+}$ (%)	$\frac{B_s^0 \rightarrow D_s^\mp K^\pm}{B^0 \rightarrow D^- \pi^+}$ (%)
All non-PID selection	2.0	2.0	3.0
PID selection	1.8	1.3	2.2
Fit model	2.4	1.7	2.2
Efficiency ratio	1.5	1.6	1.6
Total	3.9	3.4	4.6

be written as

$$\mathcal{L} = e^{-N} N^{N_{\text{obs}}} \times \prod_j G(N^j; N_c^j, \sigma_{N_0^j}) \times \prod_{i=1}^{N_{\text{obs}}} P(m_i; \vec{\lambda}), \quad (1)$$

where the first factor is the extended Poissonian likelihood in which N is the total number of fitted events, given by the sum of the fitted component yields $N = \sum_k N_k$. The fitted data sample contains N_{obs} events. The second factor is the product of the j external constraints on the yields, $j < k$, where G stands for a Gaussian PDF, and $N_c \pm \sigma_{N_0}$ is the constraint value. The third factor is a product over all events in the sample, P is the total PDF of the fit, $P(m_i; \vec{\lambda}) = \sum_k N_k P_k(m_i; \vec{\lambda}_k)$, and $\vec{\lambda}$ is the vector of parameters that define the mass shape and are not fixed in the fit.

Each simulated dataset is generated by first varying the component yield N_k using a Poissonian PDF, then sampling the resulting number of events from P_k , and repeating the procedure for all components. In addition, constraint values N_c^j used when fitting the simulated dataset are generated by drawing from $G(N; N_0^j, \sigma_{N_0^j})$, where N_0^j is the true central value of the constraint, while in the nominal fit to the data $N_c^j = N_0^j$.

The sources of systematic uncertainty considered for the fit are signal widths, the slope of the combinatorial backgrounds, and constraints placed on specific backgrounds. The largest deviations are due to the signal widths and the fixed slope of the combinatorial background in the $B_s^0 \rightarrow D_s^\mp K^\pm$ fit.

The systematic uncertainty related to PID enters in two ways: firstly as an uncertainty on the overall efficiencies and misidentification probabilities, and secondly from the shape for the misidentified backgrounds which relies on correct reweighting of PID efficiency versus momentum. The absolute errors on the individual K and π efficiencies, after reweighting of the D^{*+} calibration sample, have been determined for the momentum spectra that are relevant for this analysis, and are found to be 0.5% for $\text{DLL}_{K-\pi} < 0$ and 0.5% for $\text{DLL}_{K-\pi} > 5$.

The observed signal yields are corrected by the difference observed in the (non-PID) selection efficiencies of different modes as measured from simulated events:

$$\begin{aligned} \epsilon(B_s^0 \rightarrow D_s^- \pi^+) / \epsilon(B^0 \rightarrow D^- \pi^+) &= 1.015, \\ \epsilon(B_s^0 \rightarrow D_s^- \pi^+) / \epsilon(B_s^0 \rightarrow D_s^\mp K^\pm) &= 1.061. \end{aligned}$$

A systematic uncertainty is assigned on the ratio to account for percent level differences between the data and the simulation. These are dominated by the simulation of the hardware trigger. All sources of systematic uncertainty are summarized in Table 4.

5 Determination of the branching fractions

The $B_s^0 \rightarrow D_s^\mp K^\pm$ branching fraction relative to $B_s^0 \rightarrow D_s^- \pi^+$ is obtained by correcting the raw signal yields for PID and selection efficiency differences

$$\frac{\mathcal{B}(B_s^0 \rightarrow D_s^\mp K^\pm)}{\mathcal{B}(B_s^0 \rightarrow D_s^- \pi^+)} = \frac{N_{B_s^0 \rightarrow D_s^\mp K^\pm}}{N_{B_s^0 \rightarrow D_s^- \pi^+}} \frac{\epsilon_{B_s^0 \rightarrow D_s^- \pi^+}^{\text{PID}}}{\epsilon_{B_s^0 \rightarrow D_s^\mp K^\pm}^{\text{PID}}} \frac{\epsilon_{B_s^0 \rightarrow D_s^- \pi^+}^{\text{Sel}}}{\epsilon_{B_s^0 \rightarrow D_s^\mp K^\pm}^{\text{Sel}}}, \quad (2)$$

where ϵ_X is the efficiency to reconstruct decay mode X and N_X is the number of observed events in this decay mode. The PID efficiencies are given in Table 1, and the ratio of the two selection efficiencies is 0.943 ± 0.013 .

The ratio of the branching fractions of $B_s^0 \rightarrow D_s^\mp K^\pm$ relative to $B_s^0 \rightarrow D_s^- \pi^+$ is determined separately for the down (0.0601 ± 0.0056) and up (0.0694 ± 0.0066) magnet polarities and the two results are in good agreement. The quoted errors are purely statistical. The combined result is

$$\frac{\mathcal{B}(B_s^0 \rightarrow D_s^\mp K^\pm)}{\mathcal{B}(B_s^0 \rightarrow D_s^- \pi^+)} = 0.0646 \pm 0.0043 \pm 0.0025,$$

where the first uncertainty is statistical and the second is the total systematic uncertainty from Table 4.

The relative yields of $B_s^0 \rightarrow D_s^- \pi^+$ and $B^0 \rightarrow D^- \pi^+$ are used to extract the branching fraction of $B_s^0 \rightarrow D_s^- \pi^+$ from the following relation

$$\mathcal{B}(B_s^0 \rightarrow D_s^- \pi^+) = \mathcal{B}(B^0 \rightarrow D^- \pi^+) \frac{\epsilon_{B^0 \rightarrow D^- \pi^+}}{\epsilon_{B_s^0 \rightarrow D_s^- \pi^+}} \frac{N_{B_s^0 \rightarrow D_s^- \pi^+} \mathcal{B}(D^- \rightarrow K^+ \pi^- \pi^-)}{f_s/f_d N_{B^0 \rightarrow D^- \pi^+} \mathcal{B}(D_s^- \rightarrow K^- K^+ \pi^-)}, \quad (3)$$

using the recent f_s/f_d measurement from semileptonic decays [4]

$$\frac{f_s}{f_d} = 0.268 \pm 0.008_{-0.020}^{+0.022},$$

where the first uncertainty is statistical and the second systematic. Only the semileptonic result is used since the hadronic determination of f_s/f_d relies on theoretical assumptions about the ratio of the branching fractions of the $B_s^0 \rightarrow D_s^- \pi^+$ and $B^0 \rightarrow D^- \pi^+$ decays. In addition, the following world average values [5] for the B and D branching fractions are used

$$\begin{aligned} \mathcal{B}(B^0 \rightarrow D^- \pi^+) &= (2.68 \pm 0.13) \times 10^{-3}, \\ \mathcal{B}(D^- \rightarrow K^+ \pi^- \pi^-) &= (9.13 \pm 0.19) \times 10^{-2}, \\ \mathcal{B}(D_s^- \rightarrow K^+ K^- \pi^-) &= (5.49 \pm 0.27) \times 10^{-2}, \end{aligned}$$

leading to

$$\begin{aligned}\mathcal{B}(B_s^0 \rightarrow D_s^- \pi^+) &= (2.95 \pm 0.05 \pm 0.17_{-0.22}^{+0.18}) \times 10^{-3}, \\ \mathcal{B}(B_s^0 \rightarrow D_s^\mp K^\pm) &= (1.90 \pm 0.12 \pm 0.13_{-0.14}^{+0.12}) \times 10^{-4},\end{aligned}$$

where the first uncertainty is statistical, the second is the experimental systematics (as listed in Table 4) plus the uncertainty arising from the $B^0 \rightarrow D^- \pi^+$ branching fraction, and the third is the uncertainty (statistical and systematic) from the semileptonic f_s/f_d measurement. Both measurements are significantly more precise than the existing world averages [5].

Acknowledgments

We express our gratitude to our colleagues in the CERN accelerator departments for the excellent performance of the LHC. We thank the technical and administrative staff at CERN and at the LHCb institutes, and acknowledge support from the National Agencies: CAPES, CNPq, FAPERJ and FINEP (Brazil); CERN; NSFC (China); CNRS/IN2P3 (France); BMBF, DFG, HGF and MPG (Germany); SFI (Ireland); INFN (Italy); FOM and NWO (The Netherlands); SCSR (Poland); ANCS (Romania); MinES of Russia and Rosatom (Russia); MICINN, XuntaGal and GENCAT (Spain); SNSF and SER (Switzerland); NAS Ukraine (Ukraine); STFC (United Kingdom); NSF (USA). We also acknowledge the support received from the ERC under FP7 and the Region Auvergne.

References

- [1] R. Fleischer, *New strategies to obtain insights into CP violation through $B_s \rightarrow D_s^\pm K^\mp, D_s^{*\pm} K^\mp, \dots$ and $B_d \rightarrow D^\pm \pi^\mp, D^{*\pm} \pi^\mp, \dots$ decays*, Nucl. Phys. **B671** (2003) 459, [arXiv:hep-ph/0304027](#).
- [2] CDF collaboration, T. Aaltonen *et al.*, *First observation of $\bar{B}_s^0 \rightarrow D_s^\pm K^\mp$ and measurement of the ratio of branching fractions $B(\bar{B}_s^0 \rightarrow D_s^\pm K^\mp) / B(\bar{B}_s^0 \rightarrow D_s^\pm \pi^\mp)$* , Phys. Rev. Lett. **103** (2009) 191802, [arXiv:0809.0080](#).
- [3] Belle collaboration, R. Louvot *et al.*, *Measurement of the decay $B_s^0 \rightarrow D_s^- \pi^+$ and evidence for $B_s^0 \rightarrow D_s^\mp K^\pm$ in e^+e^- annihilation at $\sqrt{s} \sim 10.87$ GeV*, Phys. Rev. Lett. **102** (2009) 021801, [arXiv:0809.2526](#).
- [4] LHCb collaboration, R. Aaij *et al.*, *Measurement of b hadron production fractions in 7 TeV pp collisions*, Phys. Rev. D **85** (2012) 032008, [arXiv:1111.2357](#).
- [5] Particle Data Group, K. Nakamura *et al.*, *Review of particle physics*, J. Phys. **G37** (2010) 075021.

- [6] LHCb collaboration, A. A. Alves Jr. *et al.*, *The LHCb detector at the LHC*, JINST **3** (2008) S08005.
- [7] V. V. Gligorov, C. Thomas, and M. Williams, *The HLT inclusive B triggers*, LHCb-PUB-2011-016.
- [8] T. Sjöstrand, S. Mrenna, and P. Skands, *PYTHIA 6.4 Physics and manual*, JHEP **05** (2006) 026, [arXiv:hep-ph/0603175](#).
- [9] M. Clemencic *et al.*, *The LHCb Simulation Application, Gauss: Design, Evolution and Experience*, Journal of Physics: Conference Series **331** (2011), no. 3 032023.
- [10] D. J. Lange, *The EvtGen particle decay simulation package*, Nucl. Instrum. Meth. **A462** (2001) 152.
- [11] GEANT4 collaboration, S. Agostinelli *et al.*, *GEANT4: A simulation toolkit*, Nucl. Instrum. Meth. **A506** (2003) 250.
- [12] P. Golonka and Z. Was, *PHOTOS Monte Carlo: A Precision tool for QED corrections in Z and W decays*, Eur. Phys. J. **C45** (2006) 97, [arXiv:hep-ph/0506026](#).
- [13] A. Hoecker *et al.*, *TMVA: Toolkit for multivariate data analysis*, PoS **ACAT** (2007) 040, [arXiv:physics/0703039](#).
- [14] LHCb collaboration, R. Aaij *et al.*, *Determination of f_s/f_d for 7 TeV pp collisions and measurement of the $B^0 \rightarrow D^- K^+$ branching fraction*, Phys. Rev. Lett. **107** (2011) 211801, [arXiv:1106.4435](#).
- [15] T. Skwarnicki, *A study of the radiative cascade transitions between the Upsilon-prime and Upsilon resonances*. PhD thesis, Institute of Nuclear Physics, Krakow, 1986, DESY-F31-86-02.
- [16] LHCb collaboration, R. Aaij *et al.*, *Measurement of b-hadron masses*, Phys. Lett. **B708** (2012) 241, [arXiv:1112.4896](#).